

Article

Amphiphilic Poly(*N*-vinylpyrrolidone) Nanoparticles Conjugated with DR5-Specific Antitumor Cytokine DR5-B for Targeted Delivery to Cancer Cells

Anne Yagolovich ^{1,2,*}, Andrey Kuskov ³, Pavel Kulikov ⁴, Leily Kurbanova ¹, Dmitry Bagrov ², Artem Artykov ^{1,2}, Marine Gasparian ¹, Svetlana Sizova ¹, Vladimir Oleinikov ¹, Anastasia Gileva ¹, Mikhail Kirpichnikov ^{1,2}, Dmitry Dolgikh ^{1,2} and Elena Markvicheva ¹

¹ Shemyakin-Ovchinnikov Institute of Bioorganic Chemistry of the Russian Academy of Sciences, 117997 Moscow, Russia; leyli.kurbanova_1997@mail.ru (L.K.); art.al.artykov@gmail.com (A.A.); marine_gasparian@yahoo.com (M.G.); sv.sizova@gmail.com (S.S.); voleinik@mail.ru (V.O.); sumina.anastasia@mail.ru (A.G.); lemarkv@hotmail.com (E.M.); kirpichnikov@inbox.ru (M.K.); dolgikh@nmr.ru (D.D.)

² Faculty of Biology, Lomonosov Moscow State University, 119234 Moscow, Russia; bagrov@mail.bio.msu.ru

³ D. Mendeleev University of Chemical Technology of Russia, 125047 Moscow, Russia; ankuskov@mail.ru

⁴ Federal State Budgetary Institution "Centre for Strategic Planning and Management of Biomedical Health Risks" of the Federal Medical Biological Agency, 119121 Moscow, Russia; p.kulikov.p@gmail.com

* Correspondence: anneyagolovich@gmail.com



Citation: Yagolovich, A.; Kuskov, A.; Kulikov, P.; Kurbanova, L.; Bagrov, D.; Artykov, A.; Gasparian, M.; Sizova, S.; Oleinikov, V.; Gileva, A.; et al. Amphiphilic Poly(*N*-vinylpyrrolidone) Nanoparticles Conjugated with DR5-Specific Antitumor Cytokine DR5-B for Targeted Delivery to Cancer Cells. *Pharmaceutics* **2021**, *13*, 1413. <https://doi.org/10.3390/pharmaceutics13091413>

Academic Editor: Gene L. Bidwell III

Received: 31 July 2021

Accepted: 1 September 2021

Published: 7 September 2021

Publisher's Note: MDPI stays neutral with regard to jurisdictional claims in published maps and institutional affiliations.



Copyright: © 2021 by the authors. Licensee MDPI, Basel, Switzerland. This article is an open access article distributed under the terms and conditions of the Creative Commons Attribution (CC BY) license (<https://creativecommons.org/licenses/by/4.0/>).

Abstract: Nanoparticles based on the biocompatible amphiphilic poly(*N*-vinylpyrrolidone) (Amph-PVP) derivatives are promising for drug delivery. Amph-PVPs self-aggregate in aqueous solutions with the formation of micellar nanoscaled structures. Amph-PVP nanoparticles are able to immobilize therapeutic molecules under mild conditions. As is well known, many efforts have been made to exploit the DR5-dependent apoptosis induction for cancer treatment. The aim of the study was to fabricate Amph-PVP-based nanoparticles covalently conjugated with antitumor DR5-specific TRAIL (Tumor necrosis factor-related apoptosis-inducing ligand) variant DR5-B and to evaluate their *in vitro* cytotoxicity in 3D tumor spheroids. The Amph-PVP nanoparticles were obtained from a 1:1 mixture of unmodified and maleimide-modified polymeric chains, while DR5-B protein was modified by cysteine residue at the N-end for covalent conjugation with Amph-PVP. The nanoparticles were found to enhance cytotoxicity effects compared to those of free DR5-B in both 2D (monolayer culture) and 3D (tumor spheroids) *in vitro* models. The cytotoxicity of the nanoparticles was investigated in human cell lines, namely breast adenocarcinoma MCF-7 and colorectal carcinomas HCT116 and HT29. Notably, DR5-B conjugation with Amph-PVP nanoparticles sensitized resistant multicellular tumor spheroids from MCF-7 and HT29 cells. Taking into account the nanoparticles loading ability with a wide range of low-molecular-weight antitumor chemotherapeutics into hydrophobic core and feasibility of conjugation with hydrophilic therapeutic molecules by click chemistry, we suggest further development to obtain a versatile system for targeted drug delivery into tumor cells.

Keywords: poly(*N*-vinylpyrrolidone); self-assembly; nanoparticles; targeted drug delivery system; DR5 receptor; TRAIL variant DR5-B; multicellular tumor spheroids; antitumor therapy

1. Introduction

Presently, nanocarriers are increasingly developed for the treatment of solid tumors [1]. Polymeric micellar nanoparticles are of great interest due to their high stability, tunable properties and the ability for multi-drug delivery [2–4]. A number of polymeric micelles with active tumor-targeting properties were proposed for drug delivery, for example, c(RGDyK)-linked poly(carboxybetaine methacrylate)-poly(ϵ -caprolactone)-based [5], cRGD-conjugated poly(ethylene glycol)-*b*-poly(L-glutamic acid)-based [6], citric acid-functionalized poly(ϵ -caprolactone)-based micelles [7]. Poly(*N*-vinylpyrrolidone) is

non-toxic, non-carcinogenic, eco-friendly, FDA-approved biocompatible water-soluble polymer with a rather long history of pharmaceutical use [8]. Amphiphilic poly(*N*-vinylpyrrolidone) derivatives (Amph-PVP) self-aggregate in aqueous solutions with the formation of micellar nanoscaled structures, which are capable to entrap various therapeutic molecules under mild conditions [9]. The Amph-PVP nanoparticles show serum stability and excellent blood compatibility [10]. Amph-PVP tunable properties include the control of nanoparticle structure, size and morphology combined with the simple, low-cost, scalable production, making them suitable for a variety of biomedical applications [11–13], primarily drug delivery [14–16].

TRAIL is promising for targeted anticancer therapy due to its tumor selectivity and high safety profile [17]. Despite disappointing results in the first set of clinical trials, TRAIL finally passed phase III with vinorelbine and cisplatin in patients with advanced non-small-cell lung cancer, showing moderate antitumor activity [18]. TRAIL-based antitumor therapy holds promise for clinical implementation due to its tumor selectivity and safety. However, a short half-life and thus the insufficient apoptosis-inducing capacity obstruct TRAIL use in the clinic [19]. Therefore, various strategies were proposed to enhance the TRAIL stability and antitumor activity [20].

Recently, we developed TRAIL DR5 receptor-specific variant DR5-B, which has no affinity neither to DR4 nor to decoy receptors DcR1, DcR2, and osteoprotegerin and with enhanced pro-apoptotic activity in tumor cells [21]. DR5-B was shown to inhibit the growth of HCT116 colorectal cancer xenografts more efficiently compared to TRAIL and to increase animal survival [22]. The main advantage of DR5-B over the wild-type TRAIL consists in overcoming the receptor-dependent TRAIL-resistance of tumor cells. However, the pharmacokinetic parameters of DR5-B were similar to those of TRAIL, except that the DR5-B half-life was 3.5-fold higher than that one of TRAIL due to the increased selectivity to DR5 leading to lower tissue binding [22]. Thus, despite the increased DR5-B antitumor efficiency due to the DR5 specificity, its fast elimination from the body may hinder implementation to clinical practice. In spite of the development of a number of nano delivery systems for wild-type TRAIL [23], DR5-specific antitumor cytokine DR5-B has not ever been conjugated to any type of nanocarriers.

The aim of the current study was to prepare Amph-PVP-based nanoparticles covalently conjugated with DR5-specific antitumor cytokine, namely TRAIL mutant variant DR5-B, and to evaluate their *in vitro* cytotoxicity in 3D tumor spheroids. Here, we obtained new Amph-PVP-based self-assembled nanoparticles covalently conjugated with the DR5-specific antitumor cytokine DR5-B. The cytotoxicity of the nanoparticles was studied in 2D and 3D *in vitro* models using human breast adenocarcinoma MCF-7 cells, human colorectal carcinoma HCT116 and colorectal adenocarcinoma HT29 cells. To our knowledge, this is the first attempt to obtain Amph-PVP-based nanoparticles coated with the covalently linked targeted protein molecules.

2. Materials and Methods

2.1. Materials, Reagents and Cell Lines

N-vinyl-2-pyrrolidone (VP), 2,2'-azobisisobutyronitrile (AIBN), 1,4-dioxane were obtained from Acros (Geel, Belgium). Prothionamide, stearoyl chloride, maleimide, potassium tert-butyrate, dimethylsulfoxide (DMSO), fetal bovine serum (FBS), phosphate buffer saline (PBS), and all other chemicals were obtained from Sigma-Aldrich (Saint Louis, MO, USA) unless otherwise specified. All solvents and components of buffer solutions were of analytical grade and used as received. Milli-Q Plus System (Merck KGaA, Darmstadt, Germany) was used for distilled–deionized water preparation.

Human colorectal carcinoma HCT116 cells, breast adenocarcinoma MCF-7 cells, normal keratinocytes HaCaT and skin fibroblasts BJ-5ta were from ATCC (Washington, WA, USA); human colorectal adenocarcinoma HT-29 was kindly provided by Institute of Cytology, Russian Academy of Sciences (St. Petersburg, Russia). Cell culture media (DMEM, RPMI1640), 0.05% trypsin-EDTA solution, and phosphate-buffered saline tablets were from

PanEco (Moscow, Russia). Fetal bovine serum was from HyClone (Cytiva, Marlborough, MA, USA). MTT reagent was from Sigma-Aldrich (Saint Louis, MO, USA). Cyclic RGD-peptide, namely cyclo-RGDfK(TPP) for generation of multicellular tumor spheroids was kindly provided by Prof. Burov (St-Petersburg, Russia).

2.2. Expression and Purification of Recombinant Protein DR5-B

For covalent linking with Amph-PVP nanocarriers, recombinant protein DR5-B was genetically modified by replacing amino acid residue valine in 114 position to cysteine (DR5-B/V114C) by site-directed mutagenesis. The oligonucleotide primers were *ggaag-gagatatacatatgtgcagagaaagggtctc* and *gaggacctcttctctgcacatatgtatatctcctcc*. Introduction of mutations was confirmed by DNA sequencing. The highly purified recombinant protein DR5-B/V114C was obtained from *E. coli* SHuffle B strain as described previously [24]. Briefly, the cells were transformed by plasmid pET32a/sdr5-b-v114c. Cell culture was grown at 28 °C for 20 h. Cells were disrupted by French Press (Spectronic Instruments Inc., Texas City, TX, USA) under a pressure of 2000 psi. DR5-B/V114C protein was purified from the soluble fraction of cytoplasmic proteins by immobilized metal affinity chromatography on Ni-NTA agarose (Qiagen, Hilden, Germany), followed by ion-exchange chromatography on SP Sepharose (GE Healthcare, Chicago, IL, USA). Protein preparation was dialyzed against 50 mM NaH₂PO₄, 150 mM NaCl, pH 7.0 for 24 h at 4 °C, sterilized by filtration, lyophilized, and stored at −70 °C.

2.3. Production of P-DR5-B Nanoparticles

2.3.1. Synthesis of Amph-PVP-Cl (OD11000)

The amphiphilic PVP containing one end hydrophobic stearyl group was prepared by radical polymerization of monomer in dioxane with azobisisobutyronitrile as an initiator and stearyl chloride as a chain-transfer agent and chain-growth regulator, as described earlier [25]. Estimated quantities of monomer, initiator and stearyl chloride were dissolved in dioxane and polymerization reaction was carried out for 2 h at 80 °C.

Next, the obtained polymer was mixed with a five-fold volume of ultrapure water. The prepared polymer solution was purified by dialysis against ultrapure water using Slide-A-Lyzer Dialysis Cassettes (Thermo Fisher Scientific, Waltham, MA, USA) with a molecular weight cut-off (MWCO) of 12,000 Da. The medium conductivity (μS/cm) was measured every 6 and 24 h, and dialysis water was checked for impurities spectrophotometrically and by HPLC. The water was changed every 24 h. After 3 days no significant reduction of the conductivity and no presence of any impurities were observed, and the dialysis was terminated. The purified polymer solutions were subsequently freeze-dried (Martin Christ, Osterode am Harz, Germany) and used for further experiments. The yield of the polymers was about 78–89%. The number-average molecular weight (M_n) of the amphiphilic PVP was determined by functional analysis (titration) and, alternatively, in toluene solutions using vapor pressure osmometer (Knauer, Berlin, Germany) and polystyrene standards. In the current study, the obtained amphiphilic polymer with molecular weight of 11,000 Da (PVP-OD11000) was used.

2.3.2. Potassium Maleimide Synthesis

For the synthesis of potassium maleimide, a mixture of maleimide and potassium tert-butylate (with a molar excess of 1.2) was stirred at 0 °C for 1 day in the dimethoxyethane medium, followed by precipitation of potassium maleimide into dimethyl ether.

2.3.3. Modification of Amph-PVP-Cl by Maleimide Group

A maleimide group was attached to the synthesized homopolymer by reacting an amphiphilic *N*-vinyl-2-pyrrolidone homopolymer containing chlorine at the end of the hydrophilic chain (Amph-PVP-Cl) with potassium maleimide. The polymer with a maleimide active group was synthesized in the dioxane medium as follows: dry dioxane, the Amph-PVP-Cl polymer, and potassium maleimide (with a molar excess of 1.1) were stirred at

room temperature for 1 h, diluted with distilled water, dialyzed against water for 3 days and lyophilized.

2.3.4. Amph-PVP Nanoparticles Preparation

For nanoparticle preparation, various molar ratios of modified Amph-PVP-Maleimide and non-modified Amph-PVP-Cl (PVP-OD11000) polymers (1:3 and 1:1) were used. Micelles with model substance prothionamide in the hydrophobic core were prepared by an emulsification method. For this purpose, 0.4 g of the polymer mixture was dispersed in 50 mL of water and 0.005 g of prothionamide was dissolved in 2 mL of chloroform. Both solutions were mixed under ultrasonic treatment (undercooling, 12 min). After homogenization, chloroform was distilled off on a rotary evaporator Heidilph Hei-Vap Value Digital (Schwabach, Germany). To separate prothionamide which was not included in the nanoparticles, the suspension was centrifuged (4000 g, 5 min) using Sigma 4–5L (Osterode am Harz, Germany). Then the supernatant was frozen and lyophilized.

2.3.5. Conjugation of the Amph-PVP Nanoparticles with DR5-B

The DR5-B/V114C protein was conjugated with Amph-PVP nanoparticles by selective covalent interaction of the cysteine residue 114 of the protein with the Amph-PVP-Maleimide included in the nanoparticles. Conjugation was carried out in PBS (pH 7.3) at room temperature overnight, followed by centrifugation for 10 min at $10,000\times g$ and resuspension of the precipitates in PBS (pH 7.3). To determine the sorption capacity, the particles were diluted in PBS (pH 7.3) at concentration of 5 mg/mL and incubated at room temperature overnight with various amounts of the DR5-B/V114C protein. The mixtures were centrifuged for 10 min at $10,000\times g$ and the protein levels in the supernatants as well as in resuspended sediments were determined by Bradford assay.

The particle size distribution and polydispersity index (PDI) were determined by dynamic light scattering (DLS) on Brookhaven Instruments Corporation 90Plus Particle Analyzer (Holtsville, NY, USA) with 90Plus Particle Sizing Software (version 5.41, Brookhaven Instruments Corporation, Holtsville, NY, USA).

2.4. Imaging Nanoparticles by TEM and AFM

The Amph-PVP nanoparticles were imaged using transmission electron microscopy (TEM) and atomic force microscopy (AFM). For the TEM imaging, carbon-coated grids (Ted Pella, Redding, CA, USA) were treated using a glow discharge device Emitech K100X (Quorum Technologies Ltd., Lewes, UK) at 25 mA. The suspension of the nanoparticles was deposited onto the grid for 0.5–1 min, and the grids were stained with 1% uranyl acetate for 1–2 min. Images were obtained using a JEM-1011 (Jeol, Tokyo, Japan) transmission electron microscope equipped with an Orius SC1000W camera (Gatan Inc., Pleasanton, CA, USA). The acceleration voltage was at 80 kV; image processing was carried out using Fiji software [26].

For the AFM imaging, the samples were deposited onto mica sheets coated with amorphous carbon; coating was carried out using a Hitachi HUS-5GB device (Hitachi, Tokyo, Japan). As for the TEM imaging, the substrate surface was treated with a glow discharge device before sample deposition. The samples were deposited for 0.5–1 min and quickly dried with a stream of nitrogen. Imaging was carried out using a Solver PRO-M microscope (NT-MDT, Zelenograd, Russia). The images were acquired in semicontact mode with NSG10 cantilevers (nominal tip curvature radius 6 nm) at 1–1.4 Hz. Image processing was carried out using Gwyddion (version 2.53, <http://gwyddion.net/> (accessed on 7 September 2021)) [27].

2.5. Cell Culture and Multicellular Tumor Spheroids Formation

Human colorectal carcinoma HCT116 cells, human breast adenocarcinoma MCF-7 cells, human keratinocytes HaCaT and human skin fibroblasts BJ-5ta were cultured in DMEM supplemented with 10% FBS in a 5% CO₂ humidified atmosphere at 37 °C. Colorec-

tal adenocarcinoma HT-29 cells were cultured in RPMI-1640 supplemented with 10% FBS at 37 °C and 5% CO₂. The cells were detached after treatment with trypsin-EDTA solution (0.25% *v/v*), and the culture medium was replaced every 3–4 days. Multicellular tumor spheroids were produced by the RGD-induced cell self-assembly method, as described earlier [28]. Briefly, cells (50,000 cells/mL) were seeded in a 96-well plate (100 µL/well) and incubated at 37 °C for 2–3 h until the cells attached to the plate bottom. Then the medium was replaced in each well with 100 µL of complete DMEM (10% FBS) containing cyclo-RGDfK(TPP) peptide (40 µM). Finally, the cells were transferred to a CO₂ incubator, and RGD-induced spheroid formation was observed in 72 h.

2.6. Cytotoxicity Evaluation

Cytotoxicity was evaluated by MTT-assay. The tumor spheroids were generated with cyclo-RGDfK(TPP) as described in Section 2.5. Preparations at various dilutions were added to each well, and the cells were transferred to the CO₂-incubator for 24 or 48 h. After treatment, the cells were stained with a 0.05% (*w/v*) MTT solution in DMEM for 4 h. Then medium was replaced with DMSO (100 µL/well) and absorbance (570 nm) was measured by Multiskan FC reader (Thermo Fisher Scientific, Waltham, MA, USA). The cell viability was determined in % compared to the control according to the equation: (OD sample—OD background)/(OD control—OD background) × 100%. The half-maximal inhibitory concentration (IC₅₀) was determined as drug concentration resulting in 50% inhibition of cell growth.

2.7. Statistical Analysis

Cell culture experiments were repeated at least three times. The data were normally distributed and displayed as mean ± SD from at least three replicates. GraphPad Prism version 6.01 (GraphPad Software Inc, San Diego, CA, USA) for Windows was used to generate graphical representations and conduct statistical analyses of data. Comparisons between two groups from 2–3 independent experiments were made by one-way analysis of variance at 95% confidence using the unpaired *t*-test and Bonferroni's multiple comparison tests or uncorrected Fisher's least significant difference for comparisons between more than two groups. IC₅₀ values were calculated in GraphPad Prism according to the built-in dose-response inhibition formula.

3. Results

3.1. Preparation of Amph-PVP Nanoparticles

Schemes of the synthesis of compounds for the preparation of the Amph-PVP nanoparticles are shown in Figure 1. The amphiphilic *N*-vinylpyrrolidone polymers were synthesized by the originally developed one-step method reported by us earlier [25,29]. Specifically, the amphiphilic PVP containing one end stearoyl group (Amph-PVP-Cl) was prepared by radical polymerization of monomer in dioxane with azobisisobutyronitrile as an initiator and stearoyl chloride as a chain-transfer agent and chain-growth regulator (Figure 1a). Additionally, Amph-PVP-Cl molecules were modified with maleimide at the hydrophilic ends of the polymer chains for further covalent conjugation with DR5-B. For this purpose, potassium maleimide was synthesized (Figure 1b) and a maleimide group was attached to Amph-PVP-Cl by reacting with amphiphilic *N*-vinyl-2-pyrrolidone homopolymer containing chlorine at the end of the hydrophilic chain (Amph-PVP-Cl) (Figure 1c). The core of the self-assemblies was loaded with hydrophobic model substance prothionamide, an anti-tuberculosis drug without antitumor activity. Nanoparticles were obtained by the emulsion method by joint ultrasonication of prothionamide solution in chloroform and Amph-PVP solution in water.

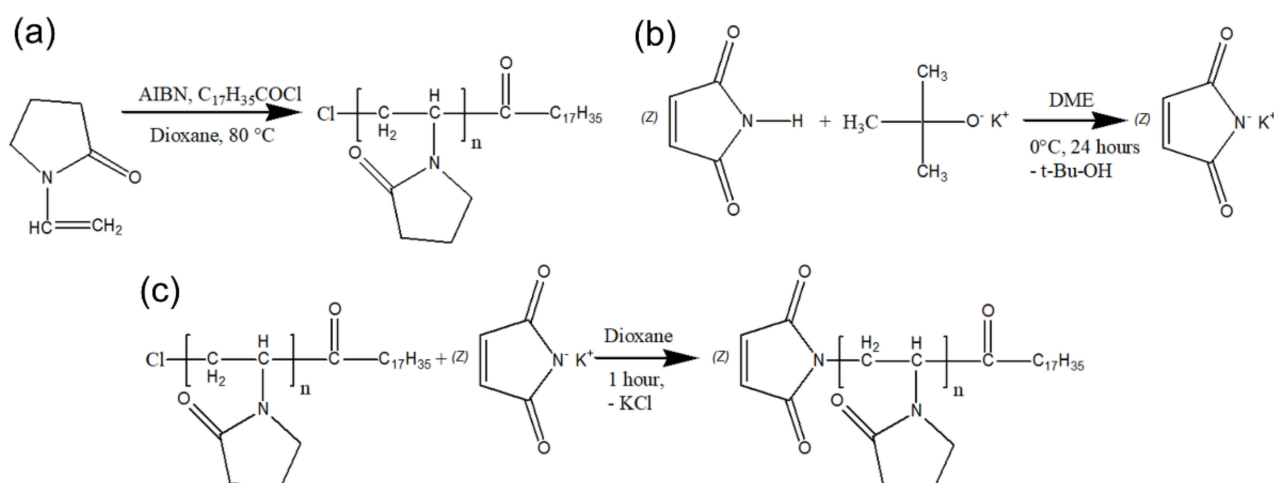


Figure 1. The synthesis schemes of compounds for further preparation of Amph-PVP nanoparticles: (a) Amph-PVP-Cl polymer; (b) potassium maleimide; (c) Amph-PVP-Cl modification by maleimide group.

We obtained two variants of self-assembled nanoparticles from mixtures of maleimide-modified and unmodified Amph-PVPs with molar ratios 1:3 and 1:1 for further optimization of the amount of the bound protein.

3.2. Conjugation of the Amph-PVP Nanoparticles with the DR5-B Protein

The DR5-B protein is the DR5 receptor-specific mutant variant of the soluble extracellular domain of TRAIL (114-281) cytokine with six amino acid substitutions. For covalent conjugation with maleimide groups of the Amph-PVP nanoparticles, the DR5-B mutant variant with N-terminal V114C substitution, namely DR5-B/V114C, was obtained by the site-specific mutagenesis. DR5-B/V114C protein in *E. coli* strain SHuffle B and purified by the recently developed method for high-throughput production of recombinant TRAIL variants, as described previously [24] (see supported data, Figure S1). The DR5-B/V114C cytotoxicity in human colorectal carcinoma HCT116 cells was similar to this one of DR5-B (Figure S2) which confirmed that N-terminal V114C substitution did not interfere with the DR5-B cytotoxic activity.

DR5-B/V114C was conjugated to the surface of the Amph-PVP nanoparticles by the selective covalent interaction of cysteine residue 114 with maleimide-modified Amph-PVP, as described in the Materials and Methods section. As a result, the DR5-B-conjugated Amph-PVP nanoparticles (further called P-DR5-B) were fabricated. Sorption capacity amounted up to 5 µg of the DR5-B protein per 1 mg of the lyophilized nanoparticles (Table 1). Expectedly, the protein sorption capacity slightly increased with an increase in maleimide-modified Amph-PVP contents. However, this dependence was non-linear, which is obviously associated with steric effects upon protein binding to the nanoparticle surface. Contents of maleimide-modified Amph-PVP and the protein attachment did not influence the nanoparticle median hydrodynamic size, which was 220 nm, as measured by DLS (Table 1, Figure 2d). Polydispersity index evidenced that both the Amph-PVP and P-DR5-B samples were unimodal (Table 1) since in both cases PDI was equal to or lower than 0.3 [30,31]. A further study was carried out with the P-DR5-B sample containing 1:1 maleimide-modified to unmodified Amph-PVP contents due to its optimal DR5-B protein sorption capacity.

Table 1. Size, polydispersity and sorption capacity of Amph-PVP-based nanoparticles depending on the polymer composition.

| Samples | P | | P-DR5-B | |
|---|-------|-------|------------|------------|
| maleimide-modified to unmodified Amph-PVPs molar ratio | 1:3 | 1:1 | 1:3 | 1:1 |
| median size, nm ¹ | 217.6 | 205.6 | 228.5 | 228.2 |
| polydispersity index ² | 0.299 | 0.302 | 0.274 | 0.303 |
| amount of DR5-B, µg per 1 mg of the lyophilized nanoparticles | - | - | 4.0 ± 0.06 | 5.0 ± 0.05 |

¹ Size was measured by DLS; mean standard deviation (SD) of size ±8.7 nm. ² Polydispersity index (PDI) was measured by DLS; mean SD of PDI ± 0.032.

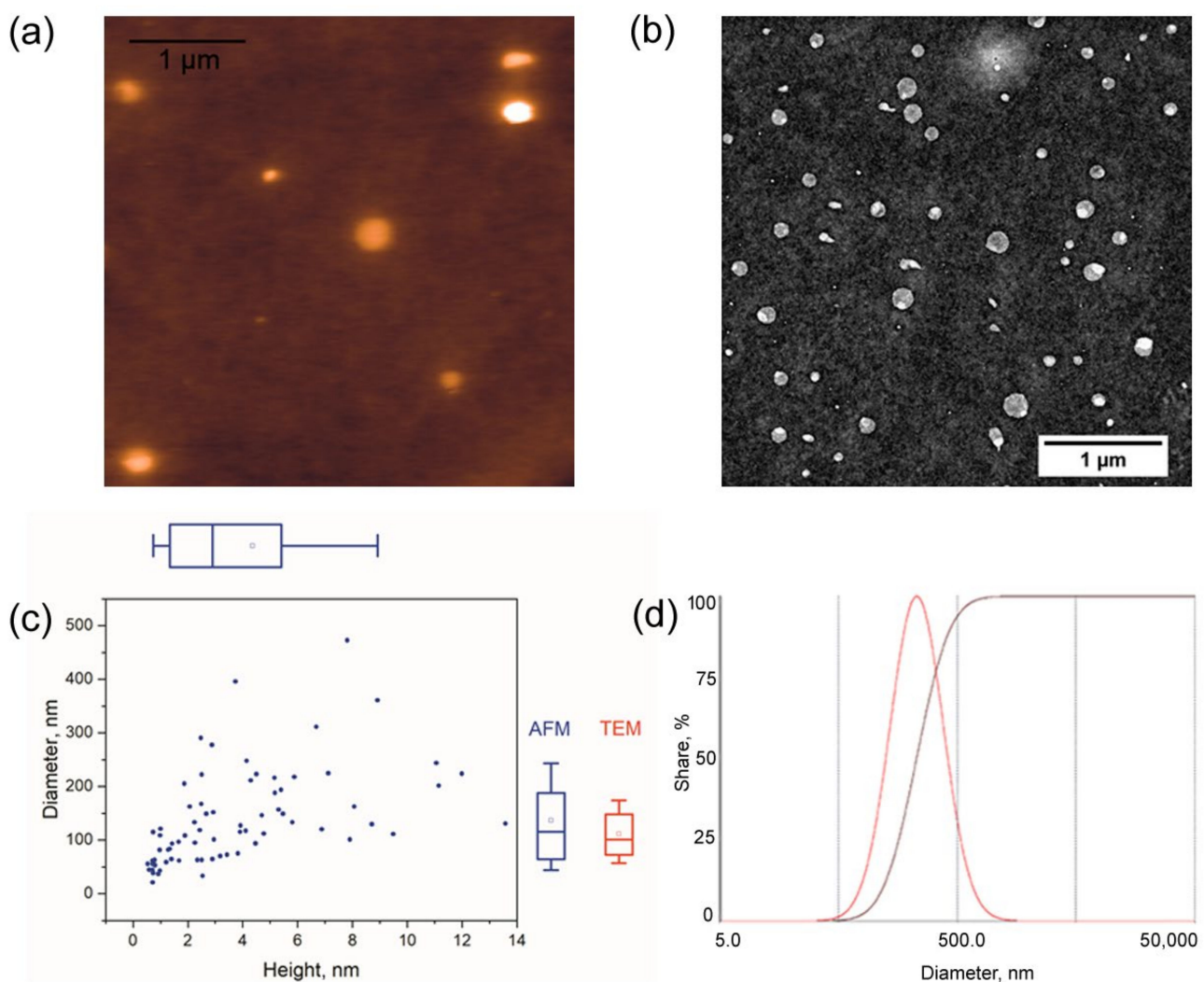


Figure 2. Characterization of DR5-B-conjugated Amph-PVP nanoparticles: (a) AFM image (Z range 15 nm); (b) TEM image; (c) diagram of the heights and widths of individual nanoparticles (blue, AFM data) and the diameters measured using TEM (in red); (d) hydrodynamic size distribution according to DLS. The box-and-whisker plots show the 10, 25, 50, 75 and 90 percentiles; the square mark shows the mean.

The P-DR5-B nanoparticles were visualized by atomic force microscopy and transmission electron microscopy (Figure 2a,b, respectively). Using both imaging techniques, we observed the round-shaped nanoparticles. We used carbon-coated mica as a substrate for the AFM imaging because upon the glow discharge treatment, it provided better sample

adsorption than the other commonly used substrates (e.g., mica or Ni²⁺-treated mica). The low height of the nanoparticles (typically below 15 nm) indicated severe flattening, as commonly observed with AFM. The diameters of individual nanoparticles measured by AFM and TEM were in good agreement, namely, the means were $D_{AFM} = 140 \pm 90$ nm and $D_{TEM} = 110 \pm 50$ nm (Figure 2c) and in a reasonable agreement with the DLS data. The median hydrodynamic size of the P-DR5-B nanoparticles measured by DLS was about 220 nm (Table 1, Figure 2d). The difference between the sizes calculated using microscopy and DLS could arise due to the sample polydispersity and the relatively low sensitivity of DLS towards the small nanoparticles.

3.3. Cytotoxicity Study of the P-DR5-B Nanoparticles in 2D and 3D In Vitro Models

The in vitro cytotoxicity of the P-DR5-B nanoparticles was evaluated in 2D (monolayer culture) and 3D (tumor spheroids) models. For this purpose, human breast adenocarcinoma MCF-7 cells, human colorectal carcinomas HCT116 cells and human colorectal adenocarcinoma HT29 cells were used. The tumor spheroids were generated by a simple RGD-induced cell self-assembly technique recently developed by the authors [28]. Expectedly, MCF-7 cells in the 2D model (Figure 3a) were more sensitive to the P-DR5-B nanoparticles compared to those in the spheroids (Figure 3b, Table 2).

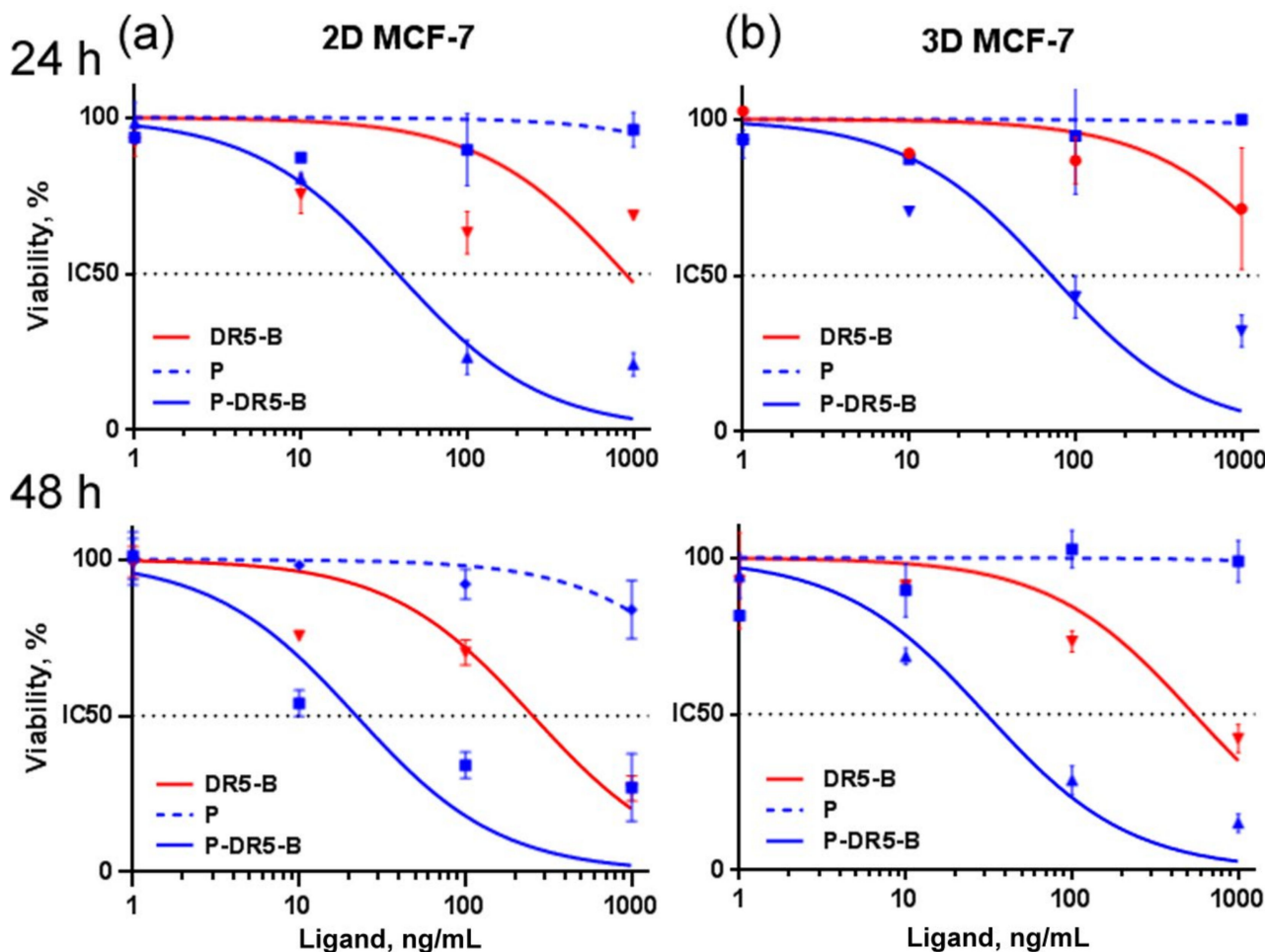


Figure 3. Cytotoxicity of the P-DR5-B nanoparticles in (a) 2D and (b) 3D human tumor models of breast adenocarcinoma MCF-7 in vitro for 24 and 48 h. Cell viability was determined by the MTT test. Mean \pm Standard Deviation ($n = 3$).

Therefore, the further cytotoxicity study of the P-DR5-B nanoparticles for HCT116 and HT29 cells were carried out only in the 3D model (Figure 4), since the spheroids are considered as a more relevant model than monolayer culture due to better mimicking

small solid tumors in vivo [32]. The P-DR5-B nanoparticles were found to surpass free DR5-B in cytotoxicity in all tested models. However, the advantage of P-DR5-B nanoparticles was more pronounced for the spheroids from DR5-B-resistant HT29 and MCF-7 cells (Figures 3b and 4b, Table 2), while in the case of the spheroids from DR5-B-sensitive HCT116 cells the cytotoxicity of the P-DR5-B nanoparticles was comparable to that of free DR5-B (Figure 4a, Table 2). The cytotoxic effect was time-dependent, increasing from 24 to 48 h of incubation (Figures 3 and 4, Table 2). Thus, conjugation of DR5-B to the nanoparticles resulted in an enhanced cell-killing capacity. The values of the standard error of the regression (S) for IC₅₀ calculations are shown in Table S1.

Table 2. IC₅₀ values (ng/mL) of free DR5-B and the P-DR5-B nanoparticles in 2D and 3D in vitro models.

| Ligand | 2D MCF-7 | | 3D MCF-7 | | 3D HCT116 | | 3D HT29 | |
|---------|----------|-------|----------|-------|-----------|-----|---------|-------|
| | 24 | 48 | 24 | 48 | 24 | 48 | 24 | 48 |
| DR5-B | 901.3 | 275.5 | >1000 | 584.0 | 16.3 | 5.0 | >1000 | 863.1 |
| P-DR5-B | 39.8 | 21.6 | 72.1 | 31.7 | 5.9 | 2.8 | 184.2 | 68.4 |

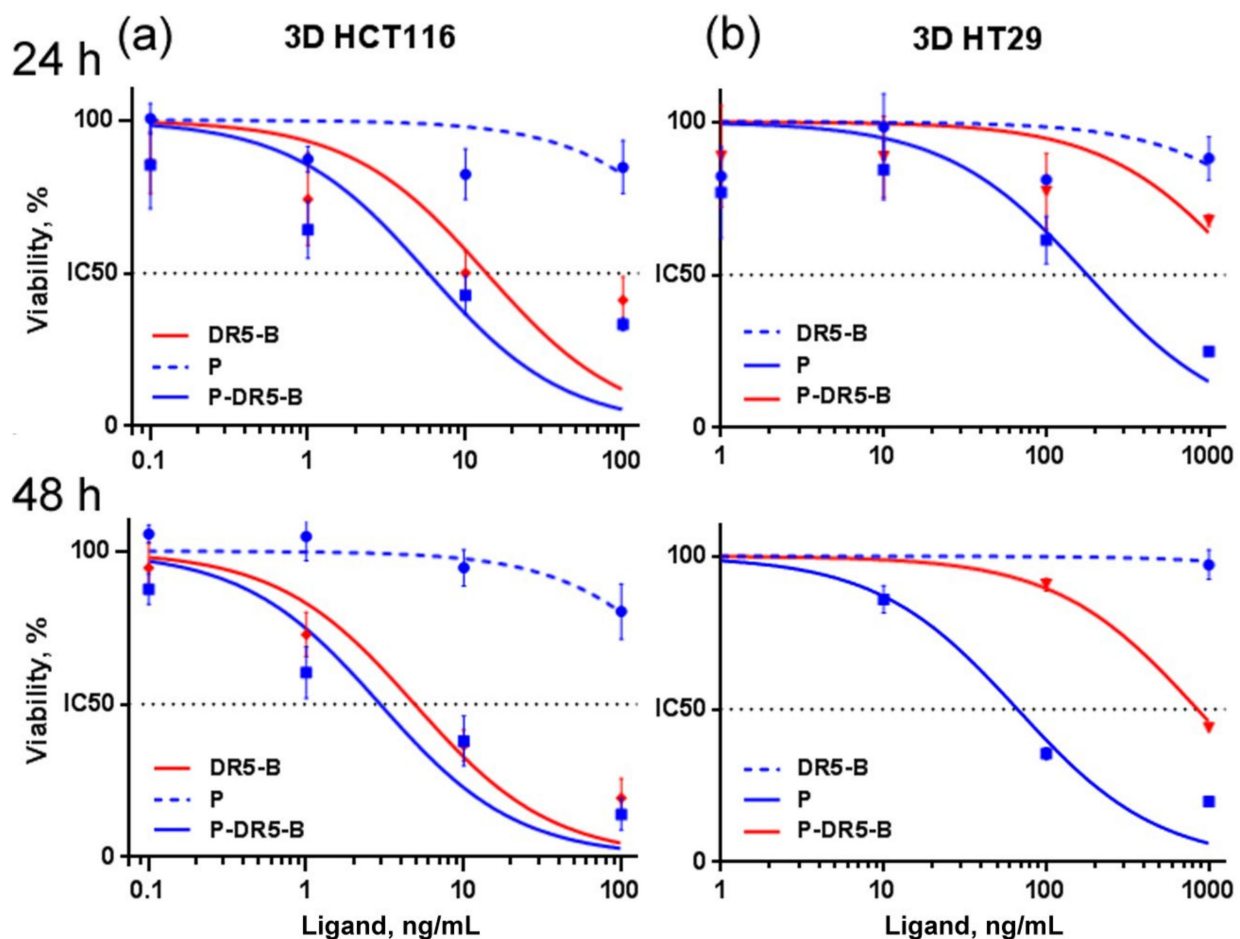


Figure 4. Cytotoxicity of the P-DR5-B nanoparticles in 3D human tumor models of (a) colorectal carcinoma HCT116; (b) colorectal adenocarcinoma HT29 in vitro for 24 and 48 h. Cell viability was determined by the MTT test. Mean \pm Standard Deviation ($n = 3$).

The morphology of 3D tumor spheroids of HCT116 colorectal carcinoma cells after incubation with P-DR5-B indicated apoptotic cell death (Figure S3).

The P-DR5-B nanoparticle's safety and tumor specificity were determined by evaluating their cytotoxicity towards normal (non-tumor) cells, namely human keratinocytes

HaCaT (Figure 5a) and human skin fibroblasts BJ-5ta (Figure 5b). Both DR5-B and blank Amph-PVP nanoparticles (without DR5-B) were non-toxic, while P-DR5-B nanoparticles were found to show a very small cytotoxic effect to BJ-5ta cells, which was beyond subtoxic values even at the maximal concentration (Figure 5a,b).

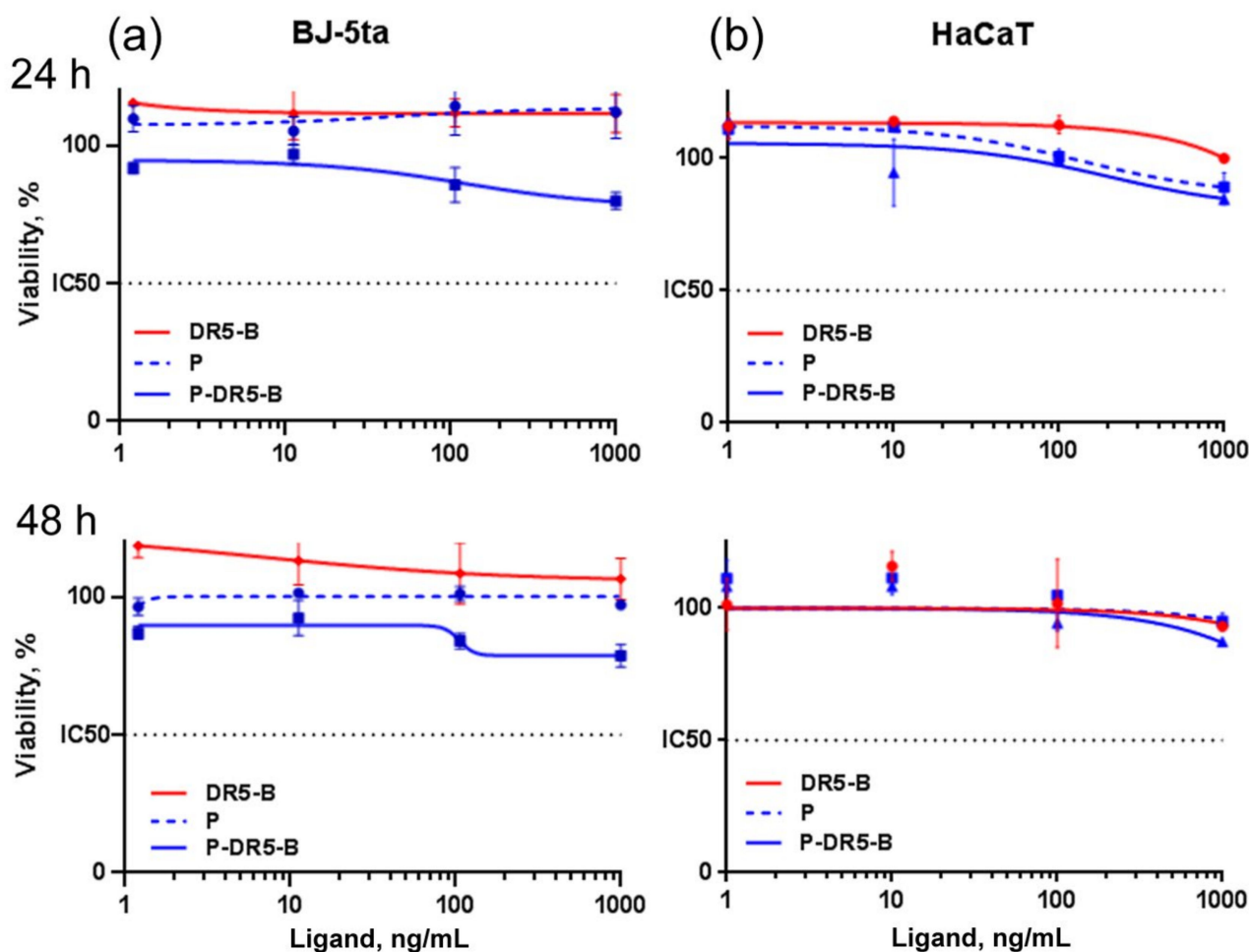


Figure 5. Cytotoxicity of the P-DR5-B nanoparticles in normal BJ-5ta (a) and HaCaT (b) cell lines after 24 and 48 h. Cell viability was determined by the MTT-test. Mean \pm Standard Deviation ($n = 3$).

4. Discussion

The versatility and the unique properties of the PVP determined its wide use for various pharmaceutical and biomedical applications. Polymers based on *N*-vinylpyrrolidone derivatives are widely used in various medical devices and preparations, including the blood-retina nanocarrier platforms [33] and bioprinting [34]. PVP is used in drug delivery systems as a coating ingredient or in nanocarriers for the delivery of low-molecular-weight and hydrophobic drugs [8,35]. PVP is well-suited for bioconjugation as a drug carrier with a narrow molecular weight distribution [36]. Recently, it was proposed as a polymeric drug carrier for bioactive protein. For example, TNF- α conjugated with PVP circulated longer than TNF- α conjugated with polyethylene glycol with the same molecular weight [37]. PVP coating of the silver nanoparticles was used to reduce Ag cytotoxicity and to enhance stability in vivo, while further conjugation to IL-10 was found to increase the protein stability and anti-inflammatory efficacy [38].

Amph-PVP-based nanocarriers were proposed for the delivery of non-steroidal anti-inflammatory drugs [39,40] and for drug delivery into the cell nucleus [41]. Moreover, amphiphilic linear-dendritic block copolymers based on the linear PVP and dendritic phenylalanyl-lysine dipeptide were reported for the enzyme-responsive release of doxoru-

bicin [42]. However, we did not find any reports, where Amph-PVP-based nanocarriers were proposed for targeted hydrophilic therapeutic macromolecules, namely targeted proteins.

At present, many efforts have been made to exploit DR5-dependent apoptosis induction for cancer treatment. TRAIL, a natural ligand for DR5, is a transmembrane protein with the N-terminal cytoplasmic domain and the C-terminal extracellular domain, which can be proteolytically cleaved from the cell surface and maintain in the body both in soluble and in membrane-associated forms. However, membrane-bound TRAIL exhibits increased activity [43]. Therefore, various nanoscale delivery systems were developed to enhance the delivery of TRAIL and other DR5-targeting molecules to cancer cells [20]. Among them, several TRAIL-based micellar systems were obtained. For example, self-assembled micellar nanoparticles from a biodegradable cationic copolymer P(MDS-*co*-CES) binding TRAIL through hydrogen bonds, hydrophobic interaction, and van der Waals forces [44]; PEG-PE (polyethylene glycol-phosphatidylethanolamine) micelles with incorporated DM-PIT-1 (*N*-{[(2-hydroxy-5-nitrophenyl)amino]carbonothioyl}-3,5-dimethylbenzamide) and TRAIL attached to the micelle surface via pNP groups [45]; self-assembled micelles from biodegradable amphiphilic copolymers, mPEG-PLA (monomethoxyl poly(ethylene glycol)-*b*-poly(DL-lactide)) and COOH-PEG-PLA, coupled with the TRAIL protein by a carbodiimide method [46]; paclitaxel loaded waterborne polyurethane nanomicelles conjugated with TRAIL through hydrogen bonds (PTX-PU-TRAIL) [47]; self-assembled amphiphilic peptide nanostructures targeting DR5 with TRAIL-mimetic DR5-targeting peptide, acting as a dual-targeting and therapeutic agent [48].

In the current study, we propose a new nanoscaled delivery system based on the Amph-PVP nanoparticles coated with the covalently attached antitumor DR5-specific cytokine DR5-B, reported by the authors earlier [21]. Despite Amph-PVPs hold a great promise for conjugation with therapeutic molecules, no attempts were made to use them as nanocarriers for TRAIL receptor agonists. Therefore, our data are absolutely new for this type of nanoscaled system.

Mostly all available TRAIL-based nanodelivery systems deal with the wild-type TRAIL, therefore they interact with all five TRAIL receptors. It was previously shown that TRAIL binding to a complicated death and decoy receptor system can lead to the activation of non-canonical signaling pathways, displaying anti-apoptotic effects [49]. Therefore, nanocarrier conjugation with the DR5-selective cytokine DR5-B allows for the avoidance of this obstacle with the advantage of overcoming the receptor-dependent resistance of tumor cells to TRAIL. Notably, specific binding of DR5-B protein to the DR5 receptor provides active tumor targeting of P-DR5-B nanoparticles.

To stabilize the Amph-PVP nanoparticles, model substance prothionamide was entrapped into the hydrophobic core. Prothionamide was chosen due to its high hydrophobicity, lack of cytotoxic activity at concentrations used and was approved for clinical application [50]. However, our further study will proceed in loading the P-DR5-B nanoparticles hydrophobic core with a number of chemotherapeutics, especially those, which showed synergistic antitumor activity with DR5-B.

To obtain the P-DR5-B nanoparticles, the DR5-B protein was modified by the cysteine amino acid residue at the N-end for further covalent conjugation with Amph-PVP. This construct has several advantages: (a) the covalent bond ensures efficient protein coupling by standard click chemistry reaction, providing construct stability at storage; (b) the correct sterical orientation of the protein molecules due to strict N-terminal conjugation of DR5-B/V114C which provides efficient DR5 receptor binding.

Due to steric hindrances along with protein conjugation to the nanoparticle surface, it was reasonable to obtain the Amph-PVP nanoparticles from a mixture of unmodified and maleimide-modified polymeric chains. To optimize the amount of the bound protein, we constructed the nanoparticles which differed in ratios of maleimide-modified to unmodified Amph-PVP polymers. Expectedly, the nanoparticles with a greater proportion of maleimide-modified Amph-PVPs coupled more DR5-B/V114C protein. However, the relation was non-linear, indicating that further increase in the maleimide-modified polymer

content may result in an insignificant increase in protein sorption capacity. Therefore the further study was carried out with the nanoparticles containing 1:1 unmodified to modified Amph-PVPs.

Our earlier works evidence that at polymer concentrations near its CMC (about 10^{-7} M) the much smaller size of the micelles (20–30 nm) can be obtained [14]. However, this is valid for plain micelles, unloaded with drugs. For drugs entrapment or immobilization on the surface of the nanoparticles, the polymers are taken in concentrations several orders higher than their CMC (10^{-6} – 10^{-4} M), when more complex aggregates of spherical morphology and larger sizes are formed [39]. The introduction of the drug into the system also influences the size of obtained nanoparticles [13,40]. Therefore, the obtained nanoparticle size (about 220 nm) correlates with our previous findings.

Cytotoxicity of the P-DR5-B nanoparticles was tested *in vitro* using 3D multicellular tumor spheroids. The tumor spheroids were generated by a simple RGD-induced cell self-assembly technique which was recently developed by us [28]. As well known, tumor spheroids are considered as a more relevant model for anticancer drug discovery compared to monolayer cultures [51], particularly for studying the antitumor activity of nanomedicines [52,53]. Due to their 3D structure, the tumor spheroids can mimic heterogeneity and microenvironment of small avascular solid tumors *in vivo*, including specific gene expression, cell-to-cell and cell-to extracellular matrix interactions, growth kinetics, metabolic rates and resistance to chemotherapy [54]. As a result, this 3D *in vitro* model allows us to get more complete information on cytotoxic effects, being an intermediate stage between 2D *in vitro* model (monolayer culture) and testing in animals. Moreover, the use of the tumor spheroids could reduce the number of animal tests, meeting the ethical rule of the 3Rs (Reduce, Replace, Refine).

In our study, the P-DR5-B nanoparticles not only retained the biological activity of free DR5-B but were also found to show enhanced antitumor activity in 2D and 3D *in vitro* models. Primarily, conjugation of TRAIL and other DR5-specific molecules with nanoscaled carriers pursues a goal to enhance ligand stability and pharmacokinetic profile, as well as to increase nanocarrier accumulation in the tumor due to enhanced permeability and retention (EPR) effect. However, it is equally important that ligand immobilization on the nanoparticle surface increases its valence and promotes DR5 receptor clustering on the tumor cell surface. Notably, the antitumor activity of the P-DR5-B nanoparticles exceeded that of free DR5-B even *in vitro*. The possible reason is that conjugation of DR5-B with the surface of the Amph-PVP nanoparticles increased its local concentration, leading to more efficient apoptosis signaling due to enhanced DR5 clustering. Recent studies support this phenomenon, demonstrating that TRAIL immobilization on the nanoparticle surface can mimic the endogenous membrane-bound form and promote high-order TRAIL oligomerization. These results related to superior DR5 clustering, enhanced DISC recruitment and more efficient apoptosis induction [43,55–59]. Further *in vivo* experiments could provide more accurate data on the pharmacokinetic profile of the P-DR5-B nanoparticles and their antitumor efficacy.

5. Conclusions

In the current study, we fabricated and characterized in terms of size and morphology novel Amph-PVP nanoparticles covalently attached to DR5-specific antitumor cytokine DR5-B for targeted delivery to tumor cells. The cytotoxic effects of the obtained P-DR5-B nanoparticles were tested both in 2D and 3D *in vitro* models using three tumor cell lines and two normal cell cultures. This nanoscaled delivery system was shown to combine advantages of the Amph-PVP nanoparticles and DR5-specific tumor targeting, together with efficient antitumor activity due to DR5-induced apoptosis induction.

Due to Amph-PVPs hydrophobic core drug-loading capacity, along with the possibility of standard click chemistry application for surface modification by therapeutic hydrophilic proteins, we can suggest that this approach is promising for the development of a versatile targeted nanoscaled delivery system.

Supplementary Materials: The following are available online at <https://www.mdpi.com/article/10.3390/pharmaceutics13091413/s1>, Figure S1: Expression and purification of DR5-B/V114C protein; Figure S2: DR5-B/V114C cytotoxic activity in colorectal carcinoma HCT116 cell line. Figure S3: Morphology of 3D tumor spheroids of HCT116 colorectal carcinoma cells after 24 h incubation with P-DR5-B at a concentration corresponding to 100 ng/mL of the DR5-B ligand. Table S1: The values of standard errors of the regression (S) for IC50 of free DR5-B and the P-DR5-B nanoparticles in 2D and 3D in vitro models.

Author Contributions: Conceptualization, A.Y. and A.K.; formal analysis, A.Y., A.K., A.G., M.G. and E.M.; funding acquisition, A.Y. and D.D.; investigation, P.K., L.K., D.B., A.A. and S.S.; methodology, A.Y., A.K., D.B. and E.M.; project administration, A.Y. and E.M.; resources, A.K., V.O., M.G. and E.M.; supervision, M.K.; validation, A.Y., M.G. and A.G.; visualization, A.Y., P.K., D.B. and A.G.; writing—original draft, A.Y., P.K. and D.B.; writing—review and editing, A.K., D.D., M.G. and E.M. All authors have read and agreed to the published version of the manuscript.

Funding: This research was funded by Russian Science Foundation grant No. 21-14-00224, <https://rscf.ru/project/21-14-00224/> (accessed on 6 September 2021) (protein expression and purification and development of 3D tumor models were held at Shemyakin-Ovchinnikov Institute of Bioorganic Chemistry of the Russian Academy of Sciences) and by the Russian Foundation for Basic Research grant № 18-34-00812 (nanoparticle synthesis and characterization were held at Department of Biomaterials, D. Mendeleev University of Chemical Technology of Russia, Faculty of Biology, Lomonosov Moscow State University, and Federal State Budgetary Institution “Centre for Strategic Planning and Management of Biomedical Health Risks” of the Federal Medical Biological Agency, Moscow, Russia).

Institutional Review Board Statement: Not applicable.

Informed Consent Statement: Not applicable.

Data Availability Statement: The data presented in this study are available on request from the corresponding author.

Acknowledgments: We are grateful to Faina Juravleva for her help with protein expression and purification. Transmission electron microscopy was performed at the User Facilities Center “Electron microscopy in life sciences” at Lomonosov Moscow State University.

Conflicts of Interest: The authors declare no conflict of interest.

References

1. Wei, Q.-Y.; Xu, Y.-M.; Lau, A.T.Y. Recent Progress of Nanocarrier-Based Therapy for Solid Malignancies. *Cancers* **2020**, *12*, 2783. [[CrossRef](#)] [[PubMed](#)]
2. Thotakura, N.; Parashar, P.; Raza, K. Assessing the Pharmacokinetics and Toxicology of Polymeric Micelle Conjugated Therapeutics. *Expert Opin. Drug Metab. Toxicol.* **2021**, *17*, 323–332. [[CrossRef](#)] [[PubMed](#)]
3. Cho, H.; Lai, T.C.; Tomoda, K.; Kwon, G.S. Polymeric Micelles for Multi-Drug Delivery in Cancer. *AAPS PharmSciTech* **2015**, *16*, 10–20. [[CrossRef](#)]
4. Ulbrich, K.; Holá, K.; Šubr, V.; Bakandritsos, A.; Tuček, J.; Zbořil, R. Targeted Drug Delivery with Polymers and Magnetic Nanoparticles: Covalent and Noncovalent Approaches, Release Control, and Clinical Studies. *Chem. Rev.* **2016**, *116*, 5338–5431. [[CrossRef](#)]
5. Lin, W.; Ma, G.; Kampf, N.; Yuan, Z.; Chen, S. Development of Long-Circulating Zwitterionic Cross-Linked Micelles for Active-Targeted Drug Delivery. *Biomacromolecules* **2016**, *17*, 2010–2018. [[CrossRef](#)]
6. Miura, Y.; Takenaka, T.; Toh, K.; Wu, S.; Nishihara, H.; Kano, M.R.; Ino, Y.; Nomoto, T.; Matsumoto, Y.; Koyama, H.; et al. Cyclic RGD-Linked Polymeric Micelles for Targeted Delivery of Platinum Anticancer Drugs to Glioblastoma through the Blood–Brain Tumor Barrier. *ACS Nano* **2013**, *7*, 8583–8592. [[CrossRef](#)]
7. Sabzi, A.; Rahmani, A.; Edalati, M.; Kahroba, H.; Dadpour, M.R.; Salehi, R.; Zarebkohan, A. Targeted Co-Delivery of Curcumin and Doxorubicin by Citric Acid Functionalized Poly (ϵ -Caprolactone) Based Micelle in MDA-MB-231 Cell. *Colloids Surf. B* **2020**, *194*, 111225. [[CrossRef](#)]
8. Waleka, E.; Stojek, Z.; Karbarz, M. Activity of Povidone in Recent Biomedical Applications with Emphasis on Micro- and Nano Drug Delivery Systems. *Pharmaceutics* **2021**, *13*, 654. [[CrossRef](#)]
9. Kuskov, A.N.; Kulikov, P.P.; Goryachaya, A.V.; Tzatzarakis, M.N.; Docea, A.O.; Velonia, K.; Shtilman, M.I.; Tsatsakis, A.M. Amphiphilic Poly-N-Vinylpyrrolidone Nanoparticles as Carriers for Non-Steroidal, Anti-Inflammatory Drugs: In Vitro Cytotoxicity and in Vivo Acute Toxicity Study. *Nanomedicine* **2017**, *13*, 1021–1030. [[CrossRef](#)]

10. Tsatsakis, A.; Stratidakis, A.K.; Goryachaya, A.V.; Tzatzarakis, M.N.; Stivaktakis, P.D.; Docea, A.O.; Berdiaki, A.; Nikitovic, D.; Velonia, K.; Shtilman, M.I.; et al. In Vitro Blood Compatibility and in Vitro Cytotoxicity of Amphiphilic Poly-*N*-Vinylpyrrolidone Nanoparticles. *Food Chem. Toxicol.* **2019**, *127*, 42–52. [[CrossRef](#)] [[PubMed](#)]
11. Villemson, A.L.; Kuskov, A.N.; Shtilman, M.I.; Galebskaya, L.V.; Ryumina, E.V.; Larionova, N.I. Interaction of Polymer Aggregates Based on Stearoyl-Poly-*N*-Vinylpyrrolidone with Blood Components. *Biochemistry* **2004**, *69*, 621–628. [[CrossRef](#)]
12. Yamskov, I.A.; Kuskov, A.N.; Babievsky, K.K.; Berezin, B.B.; Krayukhina, M.A.; Samoylova, N.A.; Tikhonov, V.E.; Shtilman, M.I. Novel Liposomal Forms of Antifungal Antibiotics Modified by Amphiphilic Polymers. *Appl. Biochem. Microbiol.* **2008**, *44*, 624–628. [[CrossRef](#)]
13. Kuskov, A.N.; Villemson, A.L.; Shtilman, M.I.; Larionova, N.I.; Tsatsakis, A.M.; Tsikalas, I.; Rizos, A.K. Amphiphilic Poly-*N*-Vinylpyrrolidone Nanocarriers with Incorporated Model Proteins. *J. Phys. Condens. Matter.* **2007**, *19*, 205139. [[CrossRef](#)]
14. Kuskov, A.N.; Shtilman, M.I.; Goryachaya, A.V.; Tashmuhamedov, R.I.; Yaroslavov, A.A.; Torchilin, V.P.; Tsatsakis, A.M.; Rizos, A.K. Self-Assembling Nanoscaled Drug Delivery Systems Composed of Amphiphilic Poly-*N*-Vinylpyrrolidones. *J. Non. Cryst. Solids* **2007**, *353*, 3969–3975. [[CrossRef](#)]
15. Basyreva, L.Y.; Voinova, E.V.; Gusev, A.A.; Mikhailchik, E.V.; Kuskov, A.N.; Goryachaya, A.V.; Gusev, S.A.; Shtilman, M.I.; Velonia, K.; Tsatsakis, A.M. Fluorouracil Neutrophil Extracellular Traps Formation Inhibited by Polymer Nanoparticle Shielding. *Mater. Sci. Eng.* **2020**, *108*, 110382. [[CrossRef](#)] [[PubMed](#)]
16. Berdiaki, A.; Perisynaki, E.; Stratidakis, A.; Kulikov, P.P.; Kuskov, A.N.; Stivaktakis, P.; Henrich-Noack, P.; Luss, A.L.; Shtilman, M.M.; Tzanakakis, G.N.; et al. Assessment of Amphiphilic Poly-*N*-Vinylpyrrolidone Nanoparticles' Biocompatibility with Endothelial Cells in Vitro and Delivery of an Anti-Inflammatory Drug. *Mol. Pharm.* **2020**, *17*, 4212–4225. [[CrossRef](#)] [[PubMed](#)]
17. Ashkenazi, A.; Pai, R.C.; Fong, S.; Leung, S.; Lawrence, D.A.; Marsters, S.A.; Blackie, C.; Chang, L.; McMurtrey, A.E.; Hebert, A.; et al. Safety and Antitumor Activity of Recombinant Soluble Apo2 Ligand. *J. Clin. Investig.* **1999**, *104*, 155–162. [[CrossRef](#)]
18. Ouyang, X.; Shi, M.; Jie, F.; Bai, Y.; Shen, P.; Yu, Z.; Wang, X.; Huang, C.; Tao, M.; Wang, Z.; et al. Phase III Study of Dulanermin (Recombinant Human Tumor Necrosis Factor-Related Apoptosis-Inducing Ligand/Apo2 Ligand) Combined with Vinorelbine and Cisplatin in Patients with Advanced Non-Small-Cell Lung Cancer. *Investig. New Drugs* **2018**, *36*, 315–322. [[CrossRef](#)] [[PubMed](#)]
19. Kelley, S.K.; Harris, L.A.; Xie, D.; DeForge, L.; Totpal, K.; Bussiere, J.; Fox, J.A. Preclinical Studies to Predict the Disposition of Apo2L/Tumor Necrosis Factor-Related Apoptosis-Inducing Ligand in Humans: Characterization of in Vivo Efficacy, Pharmacokinetics, and Safety. *J. Pharmacol. Exp. Ther.* **2001**, *299*, 31.
20. De Miguel, D.; Lemke, J.; Anel, A.; Walczak, H.; Martinez-Lostao, L. Onto Better TRAILs for Cancer Treatment. *Cell Death Differ.* **2016**, *23*, 733–747. [[CrossRef](#)] [[PubMed](#)]
21. Gasparian, M.E.; Chernyak, B.V.; Dolgikh, D.A.; Yagolovich, A.V.; Popova, E.N.; Sycheva, A.M.; Moshkovskii, S.A.; Kirpichnikov, M.P. Generation of New TRAIL Mutants DR5-A and DR5-B with Improved Selectivity to Death Receptor 5. *Apoptosis* **2009**, *14*, 778–787. [[CrossRef](#)] [[PubMed](#)]
22. Yagolovich, A.V.; Artykov, A.A.; Karmakova, T.A.; Vorontsova, M.S.; Pankratov, A.A.; Andreev-Andrievsky, A.A.; Dolgikh, D.A.; Kirpichnikov, M.P.; Gasparian, M.E. Genetically Modified DR5-Specific TRAIL Variant DR5-B Revealed Dual Antitumor and Protumoral Effect in Colon Cancer Xenografts and an Improved Pharmacokinetic Profile. *Transl. Oncol.* **2020**, *13*, 100762. [[CrossRef](#)]
23. Belkahla, H.; Herlem, G.; Picaud, F.; Gharbi, T.; Hémadi, M.; Ammar, S.; Micheau, O. TRAIL–NP Hybrids for Cancer Therapy: A Review. *Nanoscale* **2017**, *9*, 5755–5768. [[CrossRef](#)] [[PubMed](#)]
24. Yagolovich, A.V.; Artykov, A.A.; Dolgikh, D.A.; Kirpichnikov, M.P.; Gasparian, M.E. A New Efficient Method for Production of Recombinant Antitumor Cytokine TRAIL and Its Receptor-Selective Variant DR5-B. *Biochemistry* **2019**, *84*, 627–636. [[CrossRef](#)]
25. Kuskov, A.N.; Kulikov, P.P.; Luss, A.L.; Goryachaya, A.V.; Shtil'man, M.I. Preparation of Polymer Nanoparticles by Self-Assembling of Amphiphilic Poly-*N*-Vinylpyrrolidone Derivatives in Aqueous Media. *Russ. J. Appl. Chem.* **2016**, *89*, 1461–1468. [[CrossRef](#)]
26. Schindelin, J.; Arganda-Carreras, I.; Frise, E.; Kaynig, V.; Longair, M.; Pietzsch, T.; Preibisch, S.; Rueden, C.; Saalfeld, S.; Schmid, B.; et al. Fiji: An Open-Source Platform for Biological-Image Analysis. *Nat. Methods* **2012**, *9*, 676–682. [[CrossRef](#)] [[PubMed](#)]
27. Nečas, D.; Klapetek, P. Gwyddion: An Open-Source Software for SPM Data Analysis. *Open Phys. J.* **2012**, *10*, s11534–s011. [[CrossRef](#)]
28. Akasov, R.; Zaytseva-Zotova, D.; Burov, S.; Leko, M.; Dontenwill, M.; Chiper, M.; Vandamme, T.; Markvicheva, E. Formation of Multicellular Tumor Spheroids Induced by Cyclic RGD-Peptides and Use for Anticancer Drug Testing in Vitro. *Int. J. Pharm.* **2016**, *506*, 148–157. [[CrossRef](#)]
29. Kulikov, P.P.; Kuskov, A.N.; Goryachaya, A.V.; Luss, A.N.; Shtil'man, M.I. Amphiphilic Poly-*n*-Vinyl-2-Pyrrolidone: Synthesis, Properties, Nanoparticles. *Polym. Sci. Ser. D* **2017**, *10*, 263–268. [[CrossRef](#)]
30. Sadeghi, R.; Etemad, S.G.; Keshavarzi, E.; Haghshenasfard, M. Investigation of Alumina Nanofluid Stability by UV–Vis Spectrum. *Microfluid Nanofluid* **2015**, *18*, 1023–1030. [[CrossRef](#)]

31. Danaei, M.; Dehghankhold, M.; Ataei, S.; Hasanzadeh Davarani, F.; Javanmard, R.; Dokhani, A.; Khorasani, S.; Mozafari, M. Impact of Particle Size and Polydispersity Index on the Clinical Applications of Lipidic Nanocarrier Systems. *Pharmaceutics* **2018**, *10*, 57. [[CrossRef](#)]
32. Millard, M.; Yakavets, I.; Zorin, V.; Kulmukhamedova, A.; Marchal, S.; Bezdetnaya, L. Drug Delivery to Solid Tumors: The Predictive Value of the Multicellular Tumor Spheroid Model for Nanomedicine Screening. *IJN* **2017**, *12*, 7993–8007. [[CrossRef](#)]
33. Tawfik, M.; Hadlak, S.; Götze, C.; Sokolov, M.; Kulikov, P.; Kuskov, A.; Shtilman, M.; Sahel, B.A.; Henrich-Noack, P. Live In-Vivo Neuroimaging Reveals the Transport of Lipophilic Cargo Through the Blood-Retina Barrier with Modified Amphiphilic Poly-N-Vinylpyrrolidone Nanoparticles. *J. Biomed. Nanotechnol.* **2021**, *17*, 846–858. [[CrossRef](#)]
34. Ng, W.; Yeong, W.; Naing, M. Polyvinylpyrrolidone-Based Bio-Ink Improves Cell Viability and Homogeneity during Drop-On-Demand Printing. *Materials* **2017**, *10*, 190. [[CrossRef](#)]
35. Franco, P.; De Marco, I. The Use of Poly(N-Vinyl Pyrrolidone) in the Delivery of Drugs: A Review. *Polymers* **2020**, *12*, 1114. [[CrossRef](#)] [[PubMed](#)]
36. Moncalvo, F.; Martinez Espinoza, M.I.; Cellesi, F. Nanosized Delivery Systems for Therapeutic Proteins: Clinically Validated Technologies and Advanced Development Strategies. *Front. Bioeng. Biotechnol.* **2020**, *8*, 89. [[CrossRef](#)]
37. Kaneda, Y.; Tsutsumi, Y.; Yoshioka, Y.; Kamada, H.; Yamamoto, Y.; Kodaira, H.; Tsunoda, S.; Okamoto, T.; Mukai, Y.; Shibata, H.; et al. The Use of PVP as a Polymeric Carrier to Improve the Plasma Half-Life of Drugs. *Biomaterials* **2004**, *25*, 3259–3266. [[CrossRef](#)] [[PubMed](#)]
38. Baganizi, D.; Nyairo, E.; Duncan, S.; Singh, S.; Dennis, V. Interleukin-10 Conjugation to Carboxylated PVP-Coated Silver Nanoparticles for Improved Stability and Therapeutic Efficacy. *Nanomaterials* **2017**, *7*, 165. [[CrossRef](#)] [[PubMed](#)]
39. Kuskov, A.N.; Voskresenskaya, A.A.; Goryachaya, A.V.; Artyukhov, A.A.; Shtilman, M.I.; Tsatsakis, A.M. Preparation and Characterization of Amphiphilic Poly-N-Vinylpyrrolidone Nanoparticles Containing Indomethacin. *J. Mater. Sci. Mater. Med.* **2010**, *21*, 1521–1530. [[CrossRef](#)]
40. Kuskov, A.N.; Voskresenskaya, A.A.; Goryachaya, A.V.; Shtilman, M.I.; Spandidos, D.A.; Rizos, A.K.; Tsatsakis, A.M. Amphiphilic Poly-N-Vinylpyrrolidone Nanoparticles as Carriers for Non-Steroidal Anti-Inflammatory Drugs: Characterization and in Vitro Controlled Release of Indomethacin. *Int. J. Mol. Med.* **2010**, *26*, 85–94. [[CrossRef](#)]
41. Luss, A.L.; Kulikov, P.P.; Romme, S.B.; Andersen, C.L.; Pennisi, C.P.; Docea, A.O.; Kuskov, A.N.; Velonia, K.; Mezhuev, Y.O.; Shtilman, M.I.; et al. Nanosized Carriers Based on Amphiphilic Poly-N-Vinyl-2-Pyrrolidone for Intranuclear Drug Delivery. *Nanomedicine* **2018**, *13*, 703–715. [[CrossRef](#)] [[PubMed](#)]
42. Wei, J.; Lin, F.; You, D.; Qian, Y.; Wang, Y.; Bi, Y. Self-Assembly and Enzyme Responsiveness of Amphiphilic Linear-Dendritic Block Copolymers Based on Poly(N-Vinylpyrrolidone) and Dendritic Phenylalanyl-Lysine Dipeptides. *Polymers* **2019**, *11*, 1625. [[CrossRef](#)]
43. Nair, P.M.; Flores, H.; Gogineni, A.; Marsters, S.; Lawrence, D.A.; Kelley, R.F.; Ngu, H.; Sagolla, M.; Komuves, L.; Bourgon, R.; et al. Enhancing the Antitumor Efficacy of a Cell-Surface Death Ligand by Covalent Membrane Display. *Proc. Natl. Acad. Sci. USA* **2015**, *112*, 5679–5684. [[CrossRef](#)] [[PubMed](#)]
44. Lee, A.L.Z.; Dhillon, S.H.K.; Wang, Y.; Pervaiz, S.; Fan, W.; Yang, Y.Y. Synergistic Anti-Cancer Effects via Co-Delivery of TNF-Related Apoptosis-Inducing Ligand (TRAIL/Apo2L) and Doxorubicin Using Micellar Nanoparticles. *Mol. BioSyst.* **2011**, *7*, 1512. [[CrossRef](#)] [[PubMed](#)]
45. Skidan, I.; Miao, B.; Thekkedath, R.V.; Dholakia, P.; Degterev, A.; Torchilin, V. In Vitro Cytotoxicity of Novel Pro-Apoptotic Agent DM-PIT-1 in PEG-PE-Based Micelles Alone and in Combination with TRAIL. *Drug Deliv.* **2009**, *16*, 45–51. [[CrossRef](#)]
46. Feng, C.; Han, X.; Chi, L.; Sun, J.; Gong, F.; Shen, Y. Synthesis, Characterization, and in Vitro Evaluation of TRAIL-Modified, Cabazitaxel-Loaded Polymeric Micelles for Achieving Synergistic Anticancer Therapy. *J. Biomater. Sci. Polym. Ed.* **2018**, *29*, 1729–1744. [[CrossRef](#)]
47. Ajorlou, E.; Khosroushahi, A.Y.; Yeganeh, H. Novel Water-Borne Polyurethane Nanomicelles for Cancer Chemotherapy: Higher Efficiency of Folate Receptors Than TRAIL Receptors in a Cancerous Balb/C Mouse Model. *Pharm. Res.* **2016**, *33*, 1426–1439. [[CrossRef](#)] [[PubMed](#)]
48. Moyer, T.J.; Chen, F.; Toft, D.J.; Ruff, Y.; Cryns, V.L.; Stupp, S.I. Self-Assembled Peptide Nanostructures Targeting Death Receptor 5 and Encapsulating Paclitaxel As a Multifunctional Cancer Therapy. *ACS Biomater. Sci. Eng.* **2019**, *5*, 6046–6053. [[CrossRef](#)]
49. Azijli, K.; Weyhenmeyer, B.; Peters, G.J.; de Jong, S.; Kruyt, F.A.E. Non-Canonical Kinase Signaling by the Death Ligand TRAIL in Cancer Cells: Discord in the Death Receptor Family. *Cell Death Differ.* **2013**, *20*, 858–868. [[CrossRef](#)]
50. Prothionamide. *Tuberculosis* **2008**, *88*, 139–140. [[CrossRef](#)]
51. Zanoni, M.; Pignatta, S.; Arienti, C.; Bonafè, M.; Tesi, A. Anticancer Drug Discovery Using Multicellular Tumor Spheroid Models. *Expert Opin. Drug Discov.* **2019**, *14*, 289–301. [[CrossRef](#)]
52. Lazzari, G.; Couvreur, P.; Mura, S. Multicellular Tumor Spheroids: A Relevant 3D Model for the in Vitro Preclinical Investigation of Polymer Nanomedicines. *Polym. Chem.* **2017**, *8*, 4947–4969. [[CrossRef](#)]
53. Lu, H.; Stenzel, M.H. Multicellular Tumor Spheroids (MCTS) as a 3D In Vitro Evaluation Tool of Nanoparticles. *Small* **2018**, *14*, 1702858. [[CrossRef](#)] [[PubMed](#)]
54. Han, S.J.; Kwon, S.; Kim, K.S. Challenges of Applying Multicellular Tumor Spheroids in Preclinical Phase. *Cancer Cell Int.* **2021**, *21*, 152. [[CrossRef](#)]

-
55. Zakaria, A.B.; Picaud, F.; Rattier, T.; Pudlo, M.; Saviot, L.; Chassagnon, R.; Lherminier, J.; Gharbi, T.; Micheau, O.; Herlem, G. Nanovectorization of TRAIL with Single Wall Carbon Nanotubes Enhances Tumor Cell Killing. *Nano Lett.* **2015**, *15*, 891–895. [[CrossRef](#)] [[PubMed](#)]
 56. Huet, H.A.; Growney, J.D.; Johnson, J.A.; Li, J.; Bilic, S.; Ostrom, L.; Zafari, M.; Kowal, C.; Yang, G.; Royo, A.; et al. Multivalent Nanobodies Targeting Death Receptor 5 Elicit Superior Tumor Cell Killing through Efficient Caspase Induction. *mAbs* **2014**, *6*, 1560–1570. [[CrossRef](#)]
 57. De Miguel, D.; Gallego-Lleyda, A.; Ayuso, J.M.; Pejenaute-Ochoa, D.; Jarauta, V.; Marzo, I.; Fernández, L.J.; Ochoa, I.; Conde, B.; Anel, A.; et al. High-Order TRAIL Oligomer Formation in TRAIL-Coated Lipid Nanoparticles Enhances DR5 Cross-Linking and Increases Antitumour Effect against Colon Cancer. *Cancer Lett.* **2016**, *383*, 250–260. [[CrossRef](#)]
 58. Chekkat, N.; Lombardo, C.M.; Seguin, C.; Lechner, M.-C.; Dufour, F.; Nominé, Y.; De Giorgi, M.; Frisch, B.; Micheau, O.; Guichard, G.; et al. Relationship between the Agonist Activity of Synthetic Ligands of TRAIL-R2 and Their Cell Surface Binding Modes. *Oncotarget* **2018**, *9*, 15566–15578. [[CrossRef](#)]
 59. Naval, J.; de Miguel, D.; Gallego-Lleyda, A.; Anel, A.; Martinez-Lostao, L. Importance of TRAIL Molecular Anatomy in Receptor Oligomerization and Signaling. Implications for Cancer Therapy. *Cancers* **2019**, *11*, 444. [[CrossRef](#)]